SAND98-2573J

TRACER TESTS IN A FRACTURED DOLOMITE

3. ANALYSIS OF MASS TRANSFER IN SINGLE-WELL INJECTION-WITHDRAWAL TESTS

Roy Haggerty
Sean W. Fleming
Department of Geosciences,
104 Wilkinson Hall,
Oregon State University
Corvallis, OR 97331-5506.
em: haggertr@ucs.orst.edu

Lucy C. Meigs
Sean A. McKenna
Geohydrology Department,
Sandia National Laboratories,
P.O. Box 5800, MS-0735,
Albuquerque, NM 87185-0735
em: lcmeigs@nwer.sandia.gov

Submitted to Water Resources Research, December, 1998

December 20, 1998

DISCLAIMER

ABSTRACT

We investigated multiple-rate diffusion as a possible explanation for observed behavior in a suite of single-well injection-withdrawal (SWIW) tests conducted in a fractured dolomite. We first investigated the ability of a conventional double-porosity model and a multirate diffusion model to explain the data. This revealed that the multirate diffusion hypothesis/model is most consistent with all available data, and is the only model to date that is capable of matching each of the recovery curves entirely. Second, we studied the sensitivity of the SWIW recovery curves to the distribution of diffusion rate coefficients and other parameters. We concluded that the SWIW test is very sensitive to the distribution of rate coefficients, but is relatively insensitive to other flow and transport parameters such as advective porosity and dispersivity. Third, we examined the significance of the constant double-log late-time slopes (-2.1 to -2.8), which are present in several data sets. The observed late-time slopes are significantly different than would be predicted by either conventional double-porosity or single-porosity media, and are found to be a distinctive feature of multirate diffusion under SWIW test conditions. Fourth, we found that the estimated distributions of diffusion rate coefficients are very broad, with the distributions spanning a range of at least 3.6 to 5.7 orders of magnitude.

1. INTRODUCTION

The first paper in this series [*Meigs and Beauheim*, this issue] describes the field-setting, goals, design, implementation, and results of a suite of single-well injection-withdrawal (SWIW) and multi-well convergent-flow (MWCF) tracer experiments conducted in the Culebra Dolomite Member of the Rustler Formation at the Waste Isolation Pilot Plant (WIPP) Site in southeastern New Mexico. The second paper [*Altman et al.*, this issue] discusses a number of possible interpretations of the test results. They demonstrate that the SWIW recovery curves cannot be explained with a single-porosity model employing heterogeneity in hydraulic conductivity or regional drift and suggest that the breakthrough curves cannot be explained without matrix diffusion. The fourth and last paper in this series [*McKenna et al.*, this issue] examines the MWCF tracer tests that were conducted at the same locations as the SWIW tests. *McKenna et al. also* compares results obtained from the two different types of test and discusses long-term transport implications. Further information, including the complete data sets, is found in *Meigs et al.* [1998].

The effects of multiple rates of mass transfer (or "multirate" mass transfer) have been theoretically predicted in the past, and are now being observed in an increasing number of laboratory experiments: these effects have not, until now, been documented at the field-scale. In this paper, we investigated the multirate diffusion hypothesis as it relates to the SWIW tests. The hypothesis postulates that a distribution of apparent diffusion coefficients and diffusion length-scales is responsible for anomalous behavior (e.g., anomalously long tails and scale-dependent rate coefficients) in many laboratory and field tracer experiments. As such, the goals of this investigation were to (1) investigate the hypothesis that multirate diffusion could be responsible for the observed recovery behavior in the Culebra SWIW tests; (2) develop a methodology for estimating the distribution of rate coefficients responsible for the observed behavior; (3) examine whether the hypothesis and resulting model are consistent with other hard and soft data; and (4)

examine the significance of the late-time slope of the observed SWIW recovery curves, a slope which is common to data collected from several single-well and multi-well tests.

As a model of mass transfer, multirate diffusion invokes diffusion between an advection-dominated ("mobile") zone and a diffusion-dominated rock matrix ("immobile zone") that is heterogeneous at the pore-scale. The multirate diffusion model [*Haggerty and Gorelick*, 1995, 1998] is essentially a modified double-porosity model [e.g., *Neretnieks*, 1980, 1993; also see Figure 1 and Section 3] consisting of advective porosity and diffusive porosity, with diffusion of mass from one to the other described by a range of rate coefficients. There is now a growing body of literature documenting the existence, observability, and effects of multiple rates of mass transfer on solute transport in the subsurface. Multiple rates of diffusive or sorptive mass transfer are theoretically and intuitively reasonable [e.g., *Ruthven and Loughlin*, 1971; *Villermaux*, 1981; *Rao et al.*, 1982; *Cooney et al.*, 1983; *Rasmuson*, 1985; *Wu and Gschwend*, 1988; *Brusseau et al.*, 1989; *Fong and Mulkey*, 1990; *Valocchi*, 1990; *Lafolie and Hayot*, 1993; *Haggerty and Gorelick*, 1995; *Cunningham et al.*, 1997], and have now been observed and modeled in a number of laboratory experiments [e.g., *Ball and Roberts*, 1991; *Connaughton et al.*, 1993; *Pedit and Miller*, 1994, 1995; *Chen and Wagenet*, 1995, 1997; *Culver et al.*, 1997; *Werth et al.*, 1997; *Haggerty and Gorelick*, 1998; *Lorden et al.*, 1998; and others]. However, to date, there has been no reported field study that documents the effects of multirate diffusion.

2. SINGLE-WELL INJECTION-WITHDRAWAL TRACER TESTS

A suite of SWIW tracer tests was conducted in the Culebra Dolomite Member of the Rustler Formation at the Waste Isolation Pilot Plant (WIPP) Site in southeastern New Mexico [*Meigs and Beauheim*, this issue; *Meigs et al.*, 1998]. The Culebra is a 7-m-thick, variably fractured dolomite with massive and vuggy layers, and is a potential pathway to the accessible environment in the event of a radionuclide release from the WIPP. A total of three SWIW tests

were performed at two multiple-well sites, designated as the H-11 and H-19 "hydropads". SWIW tests were performed only at the central well at both hydropads. Two tests involved the injection of two tracers each and one test involved a single tracer, resulting in a total of five SWIW data sets. The SWIW tests consisted of the consecutive injection of one or more slugs of conservative tracers into the Culebra Dolomite, followed by the injection of a Culebra brine chaser (containing no tracer), and then by a resting period of approximately 18 hours. The tracers were then removed from the formation by pumping at the same well until concentration was close to or below detection levels. The majority of tracer was removed within 48 hours of pumping, but quantifiable concentrations of tracer continued to be removed for over 1000 hours (up to 50 days) at H-11 [*Meigs and Beauheim*, this issue, Figure 6]. In this paper, we will refer to the five data sets as follows: (1) the first H-19 test (SWIW1), tracer 1 as H19S1-1; (2) the first H-19 test (SWIW1), tracer 2 as H19S1-2; (3) the second H-19 test (SWIW2), only one tracer added as H19S2; (4) the H-11 test (SWIW), tracer 1 as H11-1; and (5) the H-11 test (SWIW), tracer 2 as H11-2. Details of the injected volumes, injection rates, pumping rates, etc., are given in Table 2 of *Meigs and Beauheim* [this issue].

3. MULTIRATE DIFFUSION: MATHEMATICAL MODEL

In this section, we present and discuss the mathematical model used to describe advective-dispersive solute transport with multirate diffusion. The solutions to these equations are obtained in the Laplace domain and then numerically inverted using the de Hoog algorithm [*de Hoog et al.*, 1982]; the solutions are performed sequentially for each of the injection, resting, and pumping periods. More details of the solution method are presented in Appendix A.

The multirate diffusion model is a distributed model of diffusion representing a medium with pore-scale heterogeneity in diffusive mass transfer. As conceptualized in this paper, the multirate diffusion model is similar to that described by *Cunningham et al.* [1997] and by

Haggerty and Gorelick [1998]. Figure 1 illustrates fractures and matrix (i.e., advective and diffusive porosity) in a small volume of rock, where the matrix is heterogeneous, with respect to diffusion, at spatial scales much smaller than a representative elementary volume (REV). It is assumed that this sub-REV-scale heterogeneity is replicated in approximately the same fashion everywhere in the formation.

The multirate diffusion model is a generalization of the conventional double-porosity model in that porosity is divided into two broad categories: advective porosity (where transport is dominated by advection and dispersion) and diffusive porosity (where transport is dominated by diffusion). However, in the multirate model the diffusion rate coefficient ($\alpha_d = D_d/l^2$, see below) is described by a distribution rather than a single value. The model assumes one-dimensional diffusion along a distribution of individual pathways within matrix blocks. The distribution describes the fraction of each diffusive pathway present in the rock. Although Figure 1 shows cubic matrix blocks in the model, the pathways and the blocks can be any shape, provided that each pathway is one-dimensional, homogeneous, and independent of other pathways. With these criteria, each diffusive pathway in the distribution can be modeled with a one-dimensional diffusion equation.

Variability in the diffusion rate coefficient is due to a combination of factors, including variability in at least the following: (1) matrix-block size; (2) tortuosity; (3) pore geometry; (4) restricted diffusion within pores (i.e., diffusion is slowed by small cross-sectional area of the pore); and (5) interaction with pore walls, including sorption (though the tracers employed in our experiments are believed to be non-sorbing). For further discussion on these sources of variability, see *Pedit and Miller* [1994], *Haggerty and Gorelick* [1995, 1998], and *Pignatello and Xing* [1996].

The distribution of diffusion rate coefficients may be defined in any appropriate manner, but most commonly is defined as a statistical distribution. *Culver et al.* [1997], *Cunningham et al.* [1997], and others have used a gamma distribution, while *Pedit and Miller* [1994, 1995], *Haggerty and Gorelick* [1998] and others have employed a lognormal distribution. We will

employ a lognormal distribution; for a discussion of the reasoning behind this choice, see *Haggerty and Gorelick* [1998].

The mathematical models presented here make the following important simplifications: (1) the regional gradient is negligible; (2) the formation is isotropic, confined, horizontal, homogeneous with respect to groundwater flow, and is of constant thickness. The second set of assumptions simply guarantees that flow is radially symmetric. This is much less significant for an SWIW test than for other types of tests, particularly if the first assumption is valid, because the tracer leaves the well and comes back to the well along the same path. Therefore, although the second assumption is certainly violated within the Culebra dolomite, the effects on an SWIW test are likely minimal [*Altman et al.*, this issue].

The equations for solute transport into or out of a well, in the presence of a lognormal distribution of matrix diffusion processes, is given by

$$\frac{\partial c_a}{\partial t} + \int_0^\infty b(\alpha_d) \frac{\partial \bar{c}_d(\alpha_d)}{\partial t} d\alpha_d = \frac{1}{r} \frac{\partial}{\partial r} \left(\frac{r \alpha_L |v| \partial c_a}{R_f \quad \partial r} \right) - \frac{v}{R_f} \frac{\partial c_a}{\partial r} \tag{1}$$

$$b(\alpha_d) = \frac{\beta_{tot}}{\sqrt{2\pi}\sigma_d \alpha_d} \exp\left\{ - \frac{\left[\ln(\alpha_d) - \mu_d \right]^2}{2\sigma_d^2} \right\} \tag{2a}$$

where

$$\alpha_d \equiv \frac{D_a}{l^2} \tag{2b}$$

and

$$\beta_{tot} = \frac{\phi_d R_d}{\phi_a R_a} \tag{2c}$$

and where c_a [M/L^3] is the solute concentration in the advective porosity (e.g., fractures) ; $\bar{c}_d(\alpha_d)$ [M/L^3] is the average solute concentration in the portion of the matrix associated with a particular

diffusion rate coefficient; α_d [$1/T$] is the diffusion rate coefficient described in (2b), which is continuously distributed; $b(\alpha_d)$ [-] is the PDF of diffusion rate coefficients, which we assume to be lognormal in (2a); β_{tot} [-] is the total capacity coefficient of the formation, which is the ratio of mass in the matrix to mass in the fractures at equilibrium; α_L [L] is the longitudinal dispersivity; v [L/T] is the pore-water velocity; R_a [-] is the retardation factor in the advective porosity; r [L] is the radial coordinate (positive away from well); t [T] is time elapsed since the beginning of injection of the first tracer; σ_d is the standard deviation of the log-transformed diffusion rate coefficients; μ_d is the natural log of the geometric mean of the diffusion rate coefficients; D_a [L^2/T] is the apparent diffusion coefficient in the matrix, which may be defined most simply as the product of the aqueous diffusion coefficient of the tracer and diffusive tortuosity, although this expression may be modified to incorporate processes such as immobile zone sorption; l [L] is the length of the diffusion pathway within the matrix; ϕ_d [-] is the diffusive porosity of the formation; and R_d [-] is the retardation factor due to sorption within the diffusive porosity; ϕ_a [-] is the advective porosity.

The time-derivative of the spatially averaged solute concentration in the matrix is given by

$$\frac{\partial \bar{c}_d(\alpha_d)}{\partial t} = \frac{1}{l}\int_0^l \frac{\partial c_d(\alpha_d)}{\partial t}\, dz \,, \qquad 0 < \alpha_d < \infty \tag{3a}$$

where c_d [M/L^3] is the concentration at a point within the portion of the matrix associated with a particular diffusion rate coefficient; and z [L] is the coordinate along the pathway. Note that l is a variable part of α_d, and therefore is implicitly dependent upon α_d. The concentration at a point within the portion of the matrix associated with a particular diffusion rate coefficient is given by the solution to the diffusion equation:

$$\frac{\partial c_d(\alpha_d)}{\partial t} = D_a \frac{\partial^2 c_d(\alpha_d)}{\partial z^2} \,, \qquad 0 < \alpha_d < \infty \tag{3b}$$

The boundary condition for diffusive mass transfer is that the concentration at the edge of the matrix is equal to the concentration in the mobile zone:

$$c_d(\alpha_d) = c_a \ , \qquad 0 < \alpha_d < \infty \tag{3c}$$

To solve these equations we use the approach outlined by *Haggerty and Gorelick* [1995, 1998], where we substitute a series of first-order equations for the equations in (3a) and (3b) (see Appendix A). The substitution is done in such a way that the resulting solution for c_a is mathematically identical to that which would be obtained by solving the above equations directly. The solutions are obtained in the Laplace domain and then numerically inverted to the time domain (see Appendix A).

To model the experiments for diffusion into a sphere [e.g., *Rao et al.*, 1980; *Ball and Roberts*, 1991], we also employ (1). However, equations (2a) and (3a-c) are replaced by the following four equations, respectively:

$$\beta(\alpha_d) = \beta_{tot}\delta(\alpha_d^*) \tag{4}$$

$$\frac{\partial \bar{c}_d(\alpha_d)}{\partial t} = \frac{3}{l^3}\int_0^l z^2 \frac{\partial c_d}{\partial t}\, dz \ , \qquad \alpha_d = \alpha_d^* \tag{5}$$

$$\frac{\partial c_d}{\partial t} = \frac{D_a}{z^2}\frac{\partial}{\partial z}\left(z^2 \frac{\partial c_d}{\partial z}\right) \tag{6a}$$

$$c_d = c_a \ , \quad at\ z = l \tag{6b}$$

where $\delta(\alpha_d^*)$ is the Dirac delta (α_d^* represents a single value of α_d instead of a distribution); and l is now defined as the radius of the spherical matrix block, which is a constant.

3.1. Radially Divergent Flow (Injection Period)

For each of the three parts of an SWIW test (the injection, resting, and pumping periods), the pore-water velocities, initial conditions, and boundary conditions differ. Let us first consider the injection period.

The pore-water velocity in (1) during the injection period is given by

$$v = \frac{Q_{inj}}{2\pi r \phi_a b} \tag{7}$$

where Q_{inj} $[L^3/T]$ is the injection rate; and b $[L]$ is the formation thickness. The boundary conditions for use with (1), for conditions of radially divergent flow (injection) are

$$c_a - \alpha_L \frac{\partial c_a}{\partial r} = c_{inj} \qquad at\ r = r_w \tag{8a}$$

$$\frac{\partial c_a}{\partial r} = 0 \qquad r \to \infty \tag{8b}$$

where r_w $[L]$ is the well radius and c_{inj} is the injected concentration (which may be a function of time). Equation (8a) is the flux boundary at the well accounting for dispersion and (8b) is the boundary condition at infinity during injection. Initial conditions for radially divergent flow are that concentrations in both the advective and diffusive porosities (i.e., matrix and fracture porosities) are initially zero.

The equations described in this section must be solved over all space at the end of the injection period. We solved these equations on a one-dimensional grid (since it is assumed that concentrations change only radially away from the well). The grid used 25 equally-spaced nodes and was terminated at a distance where mobile concentrations fell below 10^{-4} of injected concentration. With this number of nodes placed to the edge of the concentration field, results were insensitive to grid spacing. An independent mass balance calculation ensured all injected mass was accounted for.

3.2. No Flow (Resting Period)

After the injection period, the well is turned off. During the resting period the pore-water velocity in the formation is assumed to be zero. This is justified because velocities near a well very rapidly come to steady-state after a change in pumping rate, even though heads may continue to change for some time. This assumption is supported and discussed by *Harvey et al.* [1994]. Therefore, (1) may be simplified to

$$\frac{\partial c_a}{\partial t} + \int_0^\infty b(\alpha_d)\frac{\partial \bar{c}_d(\alpha_d)}{\partial t}\, d\alpha_d = 0 \tag{9}$$

and all other equations remain the same. In the absence of a velocity field, no boundary conditions are required. Initial conditions for the resting period are taken as the concentrations at the end of the injection period. Concentrations are solved at the end of the resting period, spatially along the grid discussed above.

3.3. Radially Convergent Flow (Pumping Period)

The pore-water velocity in (1) during the pumping period is given by

$$v = -\frac{Q_{out}}{2\pi r \phi_a b} \tag{10}$$

where Q_{out} $[L^3/T]$ is the pumping rate. We also assume that the velocity in (10) is constant because velocities quickly come to steady-state in a radial system (see reasoning in Section 3.2). The boundary conditions for use with (1), for conditions of radially convergent flow (pumping) are

$$\frac{\partial c_a}{\partial r} = 0 \qquad r = r_w \tag{11a}$$

$$c_a = 0 \qquad r \to \infty \tag{11b}$$

Initial conditions for radially convergent flow are that concentrations (both advective and diffusive) at every point on the grid (see the end of Section 3.1) are initially identical to those at the end of the resting period.

4. MODELING OF SWIW TESTS

In this section, we present two models of the SWIW tests. First, we present results from our effort to model the experiments using conventional (single-rate) diffusion into a spherical matrix block and transport assuming radial flow. Second, we show the multirate diffusion model of the experimental results. We also present results from a sensitivity analysis with the multirate diffusion model, including confidence bounds on the parameter estimates.

Parameters used by the models were defined in one of two ways: (1) values were fixed based on knowledge of the tracer tests and the Culebra geology; and (2) values were estimated by fitting the models to the data [*Meigs and Beauheim*, this issue]. All parameters that could be fixed are shown in Table 1.

Estimation of parameters was done using a nonlinear least squares algorithm [e.g., *Marquardt*, 1963]. For each data set and model of that data we found the set of parameters that minimized the sum of squared errors on the logarithm of concentrations. We estimated the natural logs of those parameters that are strictly positive-valued. For purposes of comparison, we used the root-mean square error (RMSE), defined for natural logs of concentration and corrected for the number of parameters estimated [e.g., *Bard*, 1974, p. 178]. A first-order approximation to the estimated parameter covariance matrix ($\mathbf{V}_p$) is given by [e.g., *Bard*, 1974; *Draper and Smith*, 1981]

$$\mathbf{V}_p = \sigma^2\left(\mathbf{J}^T\mathbf{J}\right)^{-1} \tag{12}$$

where σ is the replicate variance defining the uncertainty in concentration (assumed to be uniform and equal to the RMSE), and $\mathbf{J}$ is the Jacobian, which is the matrix of sensitivities of the

model output to the parameter estimates. In the analyses that follow, σ_p is the standard deviation of the estimated parameter, which is the square root of the respective diagonal from $\mathbf{V}_p$.

4.1. Conventional Double-Porosity and Radial Transport

Figure 2 shows the best obtainable fit of the conventional double-porosity model (assuming spherical diffusion) to the H19S2 and H11-1 recovery curves. Modeling of the other recovery curves are not shown for conventional double-porosity because the two attempts with H19S2 and H11-1 clearly demonstrate that a conventional double-porosity model is inadequate. The parameters estimated from these fits and the RMSEs are given in Table 2.

We used only early-time data (first 50 hours) in the inversion procedure, roughly corresponding to the advection/dispersion-dominated part of the recovery curve. This was necessary because it was found that the conventional double-porosity model could not possibly match the late-time data (see Figure 2). When matching the late-time data was attempted, other estimated parameters in the model were made physically unreasonable (e.g., advective porosity close to 100%, or dispersivity larger than several meters, close to the spatial scale of the experiment) and the estimation algorithm would fail. In dozens of scoping runs with a conventional double-porosity model, no set of parameters was able to reproduce the late-time slope of the data. For conventional double-porosity, the slope is -1.5 for times after the advectively-dominated early part of the test, and before the diffusion time-scale of approximately l^2/D_a, [*Tsang*, 1995; *Hadermann and Heer*, 1996]. At times greater than the diffusion time-scale, the double-log slope predicted for a conventional double-porosity model quickly goes to infinity (in other words, the matrix is quickly emptied of solute once the time-scale of diffusion is reached). For these reasons, we also decided not to produce confidence bounds on the parameter estimates shown in Table 2.

4.2. Multirate Diffusion and Radial Transport

Figures 3a-e show the multirate diffusion models (assuming a lognormal distribution of rate coefficients) estimated from the five SWIW recovery curves.

From these figures we note two points. First, the data of all five SWIW data sets are fit very well by the multirate diffusion model. The RMSE values (Table 3) range from 0.150 to 0.424, which are 4 to 8 times smaller than the conventional double-porosity model for the same respective SWIW data sets. This improvement over the conventional double-porosity model is achieved with one additional estimated parameter. Second, the models fit the observed recovery curves over the entire range of data, including both early and late concentrations.

The parameters estimated from these fits, their 95% confidence intervals (i.e., $2\sigma_p$), and the associated RMSEs are given in Table 3. Since the natural logarithms of positive-valued parameters were estimated, the confidence intervals are on the logs of the estimates for all parameters except μ_d. From Table 3, we note four points. First, the parameters indicate that the estimated distribution of α_d is very broad, spanning several orders of magnitude. Second, the distribution of α_d appears to be different at H-11 than at H-19. This is discussed below in more detail. Third, μ_d and σ_d have relatively small confidence intervals, while ϕ_a and α_L generally have very large confidence intervals. In particular, we note that the confidence interval on the estimate of advective porosity suggests that this parameter is essentially unestimable in an SWIW test. Conversely, σ_d appears to be particularly well-measured by this type of test. However, the terms "large" and "small" are somewhat subjective and a more detailed analysis is given in the following sections. Fourth, parameters estimated from tests at the same well (with the exception of σ_d for the H19S1-2 recovery curve) have values that are statistically the same (i.e., their confidence intervals greatly overlap).

Figure 4 shows the estimated cumulative distribution functions (CDFs) of the diffusion rate coefficient for the five models. The graph shows the cumulative matrix volume associated with a diffusion rate coefficient smaller than a given value. The variance of the estimated

distribution is large for all tests, but is somewhat larger, in general, for the H-19 tests than for the H-11 test. The estimated CDFs display 95% of the distribution spanning a range of 4.4 to 11.7 orders of magnitude. We also note that the CDFs from the H-11 and H-19 tests appear to be self-consistent, with the exception of CDF for H19S1-2, which has a different estimated σ_d than the other two at H-19 (discussed in Section 5.2).

Figure 4 contains a shaded region, indicating the portion of the CDF of diffusion rate coefficients that could be assayed (i.e., "observed") by the tracer tests. Upper and lower limits were calculated by considering the diffusive time-scale for different parts of the CDF. The diffusive time-scale is the amount of time it takes for a solute to diffuse into a particular region, and is roughly the inverse of the diffusion coefficient for a one-dimensional micropore [e.g., *Crank*, 1975]. For example, a one-dimensional micropore that is characterized by α_d of 2.3×10^{-9} s^{-1} would require approximately 4.3×10^8 s (1.20×10^5 hr) for solute to diffuse into it. Therefore, it is unreasonable to expect that such a micropore would affect a tracer test at time-scales 100 times smaller (on the order of 1200 hr, the time of the last data point in H11-1). This reasoning is consistent with arguments based on Damkohler numbers [e.g., *Bahr and Rubin*, 1987]. Therefore, we draw an approximate lower limit of the shaded zone at 2.3×10^{-9} s^{-1}. Thus, the portion of the CDF with values of α_d smaller than the shaded region corresponds to that part of the diffusive porosity that could not be assayed by the SWIW tests. A longer-duration test would be needed to "observe" that portion of the matrix.

On the other end of the time-scale spectrum, diffusive mass transfer that is very fast will be obscured by advective processes. Since we do not know the ratio of advective to diffusive porosity, it is impossible to distinguish between pores dominated by advection and small micropores into which diffusion occurs quickly. In other words, diffusive porosity that interacts very rapidly with advective porosity is indistinguishable from the advective porosity itself. Therefore, the fastest observable diffusion processes will occur at a minimum of approximately 1 percent of transport time through the system. For our system, this initial recovery time also includes the injection and resting time (a total of about 24 hr), which corresponds to α_d of

1.2×10^{-3} s^{-1}. In reality, the fastest observable diffusion process is probably slower than this, but this provides an approximate upper bound. Again, this reasoning is consistent with an argument based on the Damkohler number.

The fringes of the estimated CDFs, lying outside the bounds in Figure 4, are highly nonunique and are not supported by data. They appear on the CDF only because we have chosen, a priori, a lognormal distribution. We have the largest degree of confidence about the part of the CDF near the center of the shaded region, with decreasing confidence toward the edges.

As discussed above, the estimated CDFs suggest that 95% of the distribution is spread over 4.4 to 11.7 orders of magnitude. However, not all of this distribution is supported by data. If the unsupported portions of the CDFs are ignored, the distributions are spread over 3.6 to 5.7 orders of magnitude. This spread should be considered a minimum, as a longer-duration experiment would likely support a wider spread.

5. DISCUSSION

5.1. Sensitivity Analysis

In this subsection we discuss the sensitivity of the multirate diffusion model to the estimated parameters.

The Jacobian (sensitivity matrix of dependent variable to model parameter) can be normalized to allow comparison of parameters sensitivities through time and from one parameter to another [*Harvey et al.*, 1996]:

$$J_{ij} = \frac{p_j \partial C_i}{\sigma \partial p_j} \tag{13}$$

where J_{ij} is the sensitivity of the modeled concentration at the i^{th} time to the j^{th} parameter, C_i is the i^{th} component of the vector of normalized concentrations through time, and p_j is j^{th} component of the vector of estimated parameters. The Jacobian is a useful instrument for investigating the sensitivity of the model to the estimated parameters as a function of time [e.g., *Wagner and Harvey*, 1997], and gives insight into the correlation between estimated parameters. A large value (either positive or negative) in the Jacobian indicates that the model, at a particular time, is sensitive to a given parameter; a small value would indicate that the model is insensitive to the parameter. The parameter covariance matrix from (12) was also used to examine cross-correlation.

Plots of the columns of the Jacobians for H11-1 and H19S2 are given in Figures 5a and 5b, respectively; each is representative of the sensitivity matrices computed for other SWIW tests at their respective locations. In both plots, it is clear that the nature of all sensitivities changes significantly between the advection/dispersion- and mass transfer-dominated parts of the simulations, a transition which occurs at roughly 40 hours at the H-11 well and roughly 30 hours at H-19.

For H11-1, the sensitivity of the model to the mass transfer parameters is much larger than to the flow parameters, and increases over time. The sensitivities to dispersivity and advective porosity are small and essentially constant for times greater than 40 hours, suggesting strong correlation. Consequently, neither parameter can be estimated with any confidence. In contrast, the sensitivities of the mean and standard deviation of the distribution of log-diffusion rate coefficients are larger and increase through time. Thus, the mass transfer parameters can be estimated with a reasonable degree of confidence, provided that good data are available at late time. These conclusions are supported both by the covariances and by the confidence intervals of the estimated parameters (see Table 3).

The sensitivity matrix for H19S2 exhibits greater complexity than H11-1. First, μ_d shows a fairly high degree of correlation with ϕ_a, but the sensitivities are somewhat larger for ϕ_a than in H11-1. This is explained as follows. The largest coefficients in the distribution of diffusion rate

coefficients represent near-instantaneous mass transfer. Hence, the corresponding diffusive porosity effectively acts as part of the advective porosity (i.e., they are indistinguishable). The fraction of the distribution of diffusion rate coefficients that are large is determined in part by μ_d (larger μ_d means that the geometric mean of α_d is larger and diffusive mass transfer is faster). Therefore, μ_d determines the fraction of the diffusive porosity that is indistinguishable from advective porosity. Consequently, μ_d and ϕ_a can be strongly correlated if μ_d is relatively large (as is the case in H19S2). Nonetheless, calculated confidence limits indicate that μ_d can still be estimated with reasonable confidence, though with somewhat less confidence than in H11-1.

Second, in H19S2, the sensitivities exhibit a higher degree of scatter and numerical error. The scatter and oscillations in the sensitivity plot are due to numerical error at very low concentrations and do not have physical significance. Sensitivities are calculated numerically as derivatives, which are very sensitive to small numerical errors.

5.2. Discussion of Estimated Parameters and Comparison with Other Data

In this subsection, we will discuss the estimated parameters, their confidence intervals, and compare these values to data external to the SWIW tests.

The values of ϕ_a and α_L (see Table 3) cannot confidently be estimated by the SWIW test: both parameters have extremely large confidence intervals. In the case of ϕ_a, the confidence intervals span all possible values of advective porosity. Dispersivity has slightly smaller confidence intervals, but the confidence intervals still span all possible values. Surprisingly, however, all estimated values of both ϕ_a and α_L are in reasonable agreement with independent information. The estimated values of α_L, for example, lie within the bounds of field-scale dispersivities observed in other types of tests at similar scales [*Gelhar et al.*, 1992]. The advective porosities we estimate are within the range expected for fractured rock, and lie at the upper end of the range observed from multi-well tests in the Culebra [*McKenna et al.*, this issue].

Advective porosity and dispersivity are not estimable by an SWIW test because the flow field is reversed in the middle of the experiment. Large and small values of these two parameters result in very similar early-time breakthroughs, and the late-time breakthrough is almost completely insensitive to the parameters. In contrast, diffusion is not affected by the reversal of the flow field. Additionally, the late-time breakthrough is very sensitive to diffusive mass transfer. Consequently, the parameters describing the distribution of diffusion rate coefficients, μ_d and σ_d (discussed below), are quite estimable in an SWIW test.

The parameters μ_d and σ_d, are estimated with smaller confidence intervals relative to their range of reasonable values. Because diffusion rate coefficients can vary over an extremely wide range, 95% confidence intervals on μ_d of about $\pm$ 1 to 2, indicate a reasonable degree of confidence for this parameter. The value of $\ln(\sigma_d)$ appears to be well-estimated by the SWIW test also (with the exception of H19S1-2, which is a much shorter data set). Other than H19S1-2, the confidence intervals on $\ln(\sigma_d)$ range from ± 0.24 to ± 0.30.

The mean and standard deviation of diffusion rate coefficients were both generally larger for H-19 recovery curves than H-11 recovery curves. This corresponds well to our current understanding of the hydrogeology at the two hydropads. On the basis of advective porosities inferred from MWCF tracer tests [*McKenna et al.*, this issue], transmissivities determined for many wells at the WIPP site [*Holt*, 1997], and examination of drill core [*Holt*, 1997], it is believed that advective transport in the Culebra dolomite at the H-11 hydropad tends to be channeled along well-connected fractures that form comparatively direct flow paths. At the H-19 hydropad, advective porosity consists not only of fracture porosity but also interparticle porosity and vugs connected by microfractures, and flow thus follows a more circuitous route [*Meigs et al.*, 1998]. Mass that is advectively transported near the H-11 hydropad experiences: (1) exposure to a smaller surface area of matrix, resulting in less matrix diffusion during a given time- or space-scale of experiment and thus lower effective matrix diffusion rates; and (2) incomplete exposure to the range of porosity types, resulting in a narrower spread to the distribution of diffusion rate coefficients.

The distributions of α_d estimated from the SWIW tests appear consistent from test to test and data set to data set, with the exception of H19S1-2. The H-11 data set and the other two H-19 data sets yielded very similar values of μ_d and σ_d for tests conducted at the same well. The estimated values of μ_d and σ_d for H19S1-2 are larger and smaller, respectively, than for H19S2 and H19S1-1. The conficence interval on σ_d for H19S1-2 is large enough, however, that the value of σ_d is very uncertain. The larger uncertainty and different estimates of μ_d and σ_d at H19S1-2 may be due to two factors. First, the H19S1-2 data set is the shortest, with several hundred hours less data than the other H-19 data sets. The tracer sampled a smaller range of mass transfer time scales and is therefore insensitive to the slowest rates of mass transfer. This resulted in a larger estimated mean diffusion rate coefficient and a lower estimated standard deviation. The influence of the time-scale of the experiment on the estimated parameters was confirmed by performing a parameter estimation on a H19S1-1 data set truncated to the length of the H19S1-2 data. The resulting estimates for μ_d and σ_d from this scoping run were intermediate between those from the H19S1-1 and H19S1-2 runs.

Second, the Culebra is heterogeneous. Of the three SWIWs at H-19, the H19S1-2 injection was conducted over the smallest volume of the Culebra [*Meigs and Beauheim*, this issue]. As a result, H19S1-2 experienced the smallest amount of heterogeneity and, therefore, may be expected to have a smaller estimated σ_d.

The CDFs of diffusion rate coefficients estimated from all recovery curves are very broad. The portions of the CDFs that are supported by data span at least 3.6 to 5.7 orders of magnitude (see Section 4.2). The significance of this for long-term solute transport in the Culebra is as follows. Diffusive mass transfer results in the average solute transport velocity decreasing as a function of time. A distribution of diffusion rate coefficients means that the decrease in velocity occurs over a longer period of time than if there were a single diffusion rate coefficient. A spread in the diffusion rate coefficients of 3.6 to 5.7 orders of magnitude means that the tracer velocity will decrease over at least 4 to 6 orders of magnitude. Because this is a minimum, it is possible that the tracer velocity could decrease over an even greater range in time.

5.3. The Late-Time Slope of the Data

The SWIW data shown in Figure 3 have late-time slopes that are very nearly constant after 200 hours. Plots of the derivatives of these log-transformed data reveal that both H-11 data sets have a constant late-time slope of -2.1. The late-time slopes for H19S1-1 and H19S2 are both approximately -2.2, while the late-time slope for H19S1-2 is approximately -2.8. For all five SWIW data sets, these slopes are remarkably different from those predicted for a conventional double-porosity model. For conventional double-porosity, the slope is -1.5 for times after the advectively-dominated early part of the test, and before the diffusion time-scale of approximately l^2/D_a, [*Hadermann and Heer*, 1996]. At times greater than the diffusion time-scale, the slope predicted for a conventional double-porosity model quickly goes to infinity.

Figure 6 shows the effect of varying σ_d from 0 (conventional double-porosity) to the estimated value of 3.57 for H11-1. For the conventional double-porosity model, we see that the slope of the graph is -1.5 from approximately 100 hr to 500 hr. However, after 500 hr, the slope steepens considerably, and would ultimately go to $-\infty$ as all mass is removed from the single-rate immobile zone. For the multirate diffusion models, the late-time slopes are constant, with values of -1.9 for $\sigma_d = 2.00$, and -2.1 for $\sigma_d = 3.5$.

In all of the SWIW data sets, the late-time slope is both constant and steeper than -1.5. We ran the multirate model for a range of parameters (many are not shown), and found that the late-time slopes are always constant and steeper than -1.5 for σ_d greater than 0. In addition, data from other types of tests (e.g., MWCF tests and one-dimensional column experiments with a pulse or square-wave injection) also show straight-line recovery curves at late times with slopes greater than -1.5, and scoping runs performed on these data have required non-zero values for σ_d in order to adequately match the entire length of the recovery curve. Therefore, we suggest that a constant late-time slope steeper than -1.5 for a pulse-injection tracer test is diagnostic of multirate mass transfer. It is important to note, however, that other effects (not believed to have influenced the SWIW tests we examined) may produce slopes similar to multirate diffusion;

these include significant tracer drift, the injection well or port not being cleared of solute, or nonlinear sorption. These effects are matters for potential future research.

5.4. Conventional Double-porosity vs. Multirate Diffusion

A growing body of literature has concluded that multirate diffusion is a significant phenomenon. The majority of this literature has shown that the estimated distributions of rate coefficients have surprisingly large variances, even in relatively homogeneous media. It is not straightforward to compare the various models directly because of different mathematical formulations, but *Pedit and Miller* [1995], *Culver et al.* [1997], *Werth et al.*, [1997], *Haggerty and Gorelick* [1998], and *Lorden et al.* [1998] all found variability in mass transfer rate coefficients that span many orders of magnitude. Our study, based on field experiments, adds to this list: estimated variability in the diffusion rate coefficient spans between at least 5 orders of magnitude (see Figure 4). In our study, we find that it is impossible to fit all parts of the field data using a conventional, single-rate double-porosity model (assuming diffusion into spherical blocks). It is possible to fit the earliest data, but these data are dominated by advection rather than mass transfer.

6. CONCLUSIONS

(1) A conventional double-porosity model incorporating distributed diffusion, such as the multirate diffusion model presented here, appears necessary to represent the recovery curves in the SWIW tests in the Culebra dolomite. A conventional, single-rate double-porosity model, assuming spherical diffusion, is not able to reproduce the observed late-time slope of the data. This is a serious short-falling of the conventional double-porosity model, because the late-time data are dominated by diffusive mass transfer. The portion of the recovery curve matched well by the conventional double-porosity model is dominated by advection and dispersion.

(2) Parameter estimation and sensitivity analyses indicate that the SWIW tests in the Culebra dolomite are generally insensitive to advective porosity and dispersivity. This is due to the reversing flow field, in which the tracer goes out from the well and returns to the well along approximately the same flow path. However, the SWIW tests appear to be particularly sensitive to matrix diffusion, and from these tests it is possible to estimate a distribution of diffusion rate coefficients with a reasonable degree of reliability, although care must be taken to address the effects of data length and quality and the nonuniqueness of the estimated lognormal distribution of diffusion rates outside the assay range of a given tracer test.

(3) The distribution of diffusion rate coefficients is particularly sensitive to late-time data. In fact, the sensitivity to these parameters generally grows through time. Therefore, accurate estimation of the distribution relies on accurate concentration data in the tail of the test, where the effects of matrix diffusion dominate the effects of advection and dispersion. It is unlikely that distributions of rate coefficients can be estimated from SWIW recovery curves that either do not contain the tail concentrations, or have very low-accuracy tails.

(4) The late-time slope of the recovery curves obtained from SWIW tests in the Culebra dolomite have constant double-log slopes between -2.1 and -2.8. Late-time slopes obtained from conventional double-porosity models, however, are -1.5 before the diffusion time-scale l^2/D_a [*Hadermann and Heer*, 1996], and quickly go from -1.5 to a slope much steeper than -2.5 after the diffusion time-scale. Therefore, a constant late-time slope between -2 and -3 is apparently diagnostic of a distribution of diffusion rate coefficients.

(5) The estimated distribution of diffusion rate coefficients is very broad for the Culebra dolomite. The estimated CDFs, which assume a lognormal distribution of rate coefficients, have a standard deviation in $\ln(\alpha_d)$ from 2.56 to 6.87. The portions of these CDFs that are supported by data are spread over at least 3.6 to 5.7 orders of magnitude. Consequently, if these distributions were accurate for the entire formation, it would take approximately this many orders of magnitude in time to experience all of the mass transfer variability in the formation. Therefore, the advection velocity of a solute in the Culebra would continue to slow over at least

3.7 to 5.7 orders of magnitude in time and possibly much longer. Any experiments or modeling conducted within these time frames would need to account for a distribution of mass transfer rate coefficients in order to accurately predict advective velocities on another time-scale.

APPENDIX A: LAPLACE-DOMAIN SOLUTION

The purpose of this appendix is to derive the Laplace-domain solution for the advective-dispersive equation in radial coordinates with multirate diffusion for (a) the injection period; (b) the resting period; and (c) the pumping period.

Haggerty and Gorelick [1995, 1998] show that the solute transport and mass transfer relationships given in (1), (2a), (3a), (3b), and (3c) can be re-written as follows:

$$\frac{\partial c_a}{\partial t} + \int_0^\infty b(\alpha_m)\frac{\partial c_m(\alpha_m)}{\partial t}\,d\alpha_m = \frac{1}{r}\frac{\partial}{\partial r}\left(\frac{r\alpha_L|v|}{R_a}\frac{\partial c_a}{\partial r}\right) - \frac{v}{R_a}\frac{\partial c_a}{\partial r} \tag{A1}$$

$$b(\alpha_m) = \sum_{j=1}^{\infty} \frac{8\beta_{tot}}{\sqrt{2\pi^5}(2j\text{-}1)^2\sigma_d\alpha_m} \exp\left\{-\frac{\left[\ln\left(\frac{4\alpha_m}{\pi^2(2j\text{-}1)^2}\right) - \mu_d\right]^2}{2\sigma_d^2}\right\} \tag{A2}$$

$$c_m(\alpha_m) = \alpha_m\left[c_a - c_m(\alpha_m)\right], \quad 0 < \alpha_m < \infty \tag{A3}$$

where c_m $[M/L^3]$ is the concentration of the multirate immobile zones; $\beta(\alpha_m)$ [-] is the distribution of first-order rate coefficients; α_m $[1/T]$ is the first-order (multirate) rate coefficient; and all other parameters are exactly as previously defined. The same boundary conditions apply as discussed in Sections 3.1-3.3. The boundary condition given in (3c) has no equivalent in the above equations, but is dealt with implicitly. Using equations (A1)-(A3) is completely equivalent in every way to using equations (1) through (3c). However, it should be noted that the immobile concentrations c_m are only mathematical constructs, and are used solely for the

purpose of "storing" mass. The advantage of using equations (A1)-(A3) is that they are mathematically simpler to use, and eliminate the need to solve many diffusion equations for concentrations within a distribution of immobile zones (each of which would need to be discretized using finite differences, finite elements, etc.) For a more complete description of this approach to solving a multirate diffusion problem, see *Haggerty and Gorelick* [1995, 1998].

We solve for concentrations after the injection period, resting period, and during the pumping period by converting (A1)-(A3) to the Laplace domain. The solution to the differential equation(s) is found in the Laplace domain, and then concentrations are obtained by inverting numerically to the time domain. Similar and related solutions have been documented extensively by *Chen* [1985], *Chen and Woodside* [1988], *Harvey et al.* [1994]; *Haggerty and Gorelick* [1995, 1998]. Therefore, we will give only the solutions in the Laplace domain, and not the derivation. A FORTRAN code was constructed to solve this problem and to estimate the parameters of the distribution of diffusion rate coefficients for SWIW tests and for multi-well tracer tests. The code is called STAMMT-R (Solute Transport And Multirate Mass Transfer in Radial coordinates) (*Haggerty et al.*, 1999). The code has undergone QA qualification at Sandia National Laboratories.

The solution in the Laplace domain to (A1)-(A3) during the injection period can be expressed nondimensionally as

$$\overline{C_a} = \overline{C_{inj}} \exp\left(\frac{\rho - \rho_0}{2}\right) \frac{\mathrm{Ai}\left(\mathcal{P}^{1/3} y\right)}{\frac{1}{2}\mathrm{Ai}\left(\mathcal{P}^{1/3} y_0\right) - \mathcal{P}^{1/3}\mathrm{Ai}'\left(\mathcal{P}^{1/3} y_0\right)} \tag{A4}$$

where

$$y = \rho + \frac{1}{4\mathcal{P}} \tag{A5}$$

$$\mathcal{P} = s\left[1 + \int_0^\infty \frac{b(\omega_m)\,\omega_m}{s + \omega_m} d\omega_m\right] \tag{A6}$$

$$T = \frac{Q_{inj} t}{2\pi b \phi_a \alpha_L^2 R_a} \tag{A7}$$

$$\omega_m = \alpha_m \frac{2\pi b \phi_a \alpha_L^2 R_a}{Q_{inj}} \tag{A8}$$

$$\rho = \frac{r}{\alpha_L} \tag{A9}$$

and where s is the Laplace parameter, an overbar denotes the Laplace transform of a variable, Ai'(*) is the derivative of the Airy function, ρ_w indicates the value of ρ at $r = r_w$, and y_0 indicates the value of y at $\rho = \rho_w$. The injected concentrations (c_{inj}) also must be transformed into the Laplace domain, as indicated in (A4). Although it is a simple matter to use a non-uniform injected concentration, we assume that injected concentrations begin at zero, then go instantaneously to a uniform value for a given pulse length, and then instantaneously return to zero. The Laplace transform of this square wave, which can be directly substituted into (A4) is

$$\overline{c_{inj}} = c_{inj} \frac{\exp\left(s\, T_{inj,i}\right) - \exp\left(s\, T_{inj,i-1}\right)}{s} \tag{A10}$$

where $T_{inj,\,i}$ refers to the dimensionless time elapsed until the end of injection of the i^{th} tracer (or chaser), and $T_{inj,\,i-1}$ refers to the dimensionless time elapsed until the end of injection of the (i-1) tracer (or chaser). Times are nondimensionalized in the same way as in (A7). For our purposes, we do not bother nondimensionalizing concentration as its nondimensional form does not change the solution.

The solution in the Laplace domain to (A1)-(A3) during the resting period can be expressed without need to nondimensionalize as

$$\overline{c_a} = \frac{c_a' + \int_0^\infty \frac{b(\alpha_m)\,\alpha_m}{s+\alpha_m} c_m'(\alpha_m)\,d\alpha_m}{s\left[1 + \int_0^\infty \frac{b(\alpha_m)\,\alpha_m}{s+\alpha_m}\,d\alpha_m\right]} \tag{A11}$$

and

$$\overline{c_m(\alpha_m)} = \frac{\alpha_m}{s+\alpha_m}\overline{c_a} + \frac{c_m'(\alpha_m)}{s+\alpha_m} \tag{A12}$$

where the concentrations with a prime (') indicate the concentration in that location at the beginning of the resting period. Concentrations are inverted at times defined since the beginning of the resting period.

The solution in the Laplace domain to (A1)-(A3) during the pumping period can be expressed nondimensionally as

$$\overline{c_a} = \exp\left(-\frac{\rho_w}{2}\right) \int_{\rho_w}^\infty \xi \exp\left(\frac{\xi}{2}\right) \mathcal{F}(\xi)\, g_1(\rho, s, \xi)\, d\xi \tag{A13}$$

where T is redefined as

$$T = \frac{Q_{out}\left(t - t_{rest} - \sum_{i=1}^{N} t_{inj,i}\right)}{2\pi b \phi_a \alpha_L^2 R_a} \tag{A14}$$

where N is the number of tracer and chaser injections (i.e., the time term is the time since the end of the rest period). Variables in (A13) are defined as follows:

$$\mathcal{F}(\rho) = c_a'(\rho) + \int_0^\infty \frac{b(\omega_m)\,\omega_m}{s+\omega_m} c_m'(\omega_m, \rho)\, d\omega_m \tag{A15}$$

$$g_1 = \frac{\pi}{\mathcal{P}^{1/3}} \mathrm{Ai}\left(\mathcal{P}^{1/3}\Lambda\right)\left[\mathrm{Bi}\left(\mathcal{P}^{1/3}y_0\right) - X\,\mathrm{Ai}\left(\mathcal{P}^{1/3}y_0\right)\right] \tag{A16}$$

$$X = \frac{\mathcal{P}^{1/3}\,\mathrm{Bi}'\left(\mathcal{P}^{1/3}y_0\right) - \frac{1}{2}\mathrm{Bi}\left(\mathcal{P}^{1/3}y_0\right)}{\mathcal{P}^{1/3}\,\mathrm{Ai}'\left(\mathcal{P}^{1/3}y_0\right) - \frac{1}{2}\mathrm{Ai}\left(\mathcal{P}^{1/3}y_0\right)} \tag{A17}$$

$$\Lambda = \xi + \frac{1}{4\mathcal{P}} \tag{A18}$$

and all other variables are as defined previously.

ACKNOWLEDGMENTS

Funding for this work was provided by Sandia National Laboratories. Sandia is a multiprogram laboratory operated by Sandia Corporation, a Lockheed Martin Company, for the United States Department of Energy under Contract DE-AC04-94AL85000. Computer resources for this work were provided by Oregon State University to RH. The authors would like to thank Michael Kelley, Yvonne Tsang, Toya Jones, Joanna Ogintz, Charles Tilburg, and Jim McCord for their assistance with various stages of this work, and also Vince Tidwell and Tom Corbet for helpful review comments.

REFERENCES

Altman, S. J., L. C. Meigs, and T. L. Jones, Tracer tests in a fractured dolomite, 2. Controls on mass recovery rates in a single-porosity system, *Water Resour. Res., this issue.*

Bahr, J. M., and J. Rubin, Direct comparison of kinetic and local equilibrium formulations for solute transport affected by surface reactions, *Water Resour. Res., 23*(3), 438-452, 1987.

Ball, W. P., and P. V. Roberts, Long-term sorption of halogenated organic chemicals by aquifer material. 2. Intraparticle diffusion. *Environ. Sci. Technol. 25*(7), 1237-1249, 1991.

Bard, Y., *Nonlinear Parameter Estimation*, Academic Press, New York, 1974.

Brusseau, M. L., R. E. Jessup, and P. S. C. Rao, Modeling the transport of solutes influenced by multiprocess nonequilibrium. *Water Resour. Res., 25*(9), 1971-1988, 1989.

Chen, C.-S., Analytical and approximate solutions to radial dispersion from an injection well to a geological unit with simultaneous diffusion into adjacent strata, *Water Resour. Res., 21*(8), 1069-1076, 1985.

Chen, C.-S., and G. D. Woodside, Analytical solution for aquifer decontamination by pumping, *Water Resour. Res., 24*(8), 1329-1338, 1988.

Chen, W., and R. J. Wagenet, Solute transport in porous media with sorption-site heterogeneity, *Environ. Sci. Technol., 29*(11), 2725-2734, 1995.

Chen, W., and R. J. Wagenet, Description of atrazine transport in soil with heterogeneous nonequilibrium sorption, *Soil Sci. Soc. Am J., 61*(2), 360-371, 1997.

Connaughton, D. F., J. R. Stedinger, L. W. Lion, and M. L. Shuler, Description of time-varying desorption kinetics: Release of naphthalene from contaminated soils, *Environ. Sci. Technol., 27*(12), 2397-2403, 1993.

Cooney, D. O., B. A. Adesanya, and A. L. Hines, Effect of particle size distribution on adsorption kinetics in stirred batch systems, *Chem. Eng. Sci., 38*(9), 1535-1541, 1983.

Crank, J., *The Mathematics of Diffusion*, 2nd ed., Oxford University Press, New York, 1975.

Culver, T. B., S. P. Hallisey, D. Sahoo, J. J. Deitsch, and J. A. Smith, Modeling the desorption of organic contaminants from long-term contaminated soil using distributed mass transfer rates, *Environ. Sci. Technol., 31*(6), 1581-1588, 1997.

Cunningham, J. A., C. J. Werth, M. Reinhard, and P. V. Roberts, Effects of grain-scale mass transfer on the transport of volatile organics through sediments, 1. Model development, *Water Resour. Res., 33*(12), 2713-2726, 1997.

de Hoog, F. R., J. H. Knight, and A. N. Stokes, An improved method for numerical inversion of Laplace transforms. *SIAM J. Sci. Stat. Comp. 3*(3), 357-366, 1982.

Draper, N. R., and H. Smith, *Applied Regression Analysis*, 2nd ed., John Wiley Sons, New York, 1981.

Fong, F. K., and L. A. Mulkey, Solute transport in aggregate media: Aggregated size distribution and mean radii, *Water Resour. Res., 26*(6), 1291-1303, 1990.

Gelhar, L. W., C. Welty, and K. R. Rehfeldt, A critical review of data on field-scale dispersion in aquifers, *Water Resour. Res., 28*(7), 1955-1974, 1992.

Hadermann, J., and W. Heer, The Grimsel (Switzerland) migration experiment: integrating field experiments, laboratory investigations and modelling, *J. Contam. Hydrol., 21*, 87-100, 1996.

Haggerty R., S. W. Fleming, and S. M. McKenna, *STAMMT-R, Solute Transport And Multirate Mass Transfer in Radial coordinates*: A FORTRAN code for modeling and analyzing radial single-well and two-well tracer tests in formations exhibiting multiple rates of diffusive mass transfer, SAND99-XXXX, Sandia National Laboratories, Albuquerque, NM, 1999 (in review).

Haggerty, R., and S. M. Gorelick, Multiple-rate mass transfer for modeling diffusion and surface reactions in media with pore-scale heterogeneity, *Water Resour. Res., 31*(10), 2383-2400, 1995.

Haggerty, R., and S. M. Gorelick, Modeling mass transfer processes in soil columns with pore-scale heterogeneity, *Soil Sci. Soc. Am. J., 62*(1), 62-74, 1998.

Harvey, C. F., R. Haggerty, and S. M. Gorelick, Aquifer remediation: A method for estimating mass transfer rate coefficients and an evaluation of pulsed pumping, *Water Resour. Res., 30*(7), 1979-1991, 1994.

Harvey, J.W., B. J., Wagner, and K. E. Bencala, Evaluating the reliability of the stream tracer approach to characterize stream-subsurface water exchange, *Water Resour. Res., 32*(8), 2441-2451, 1996.

Holt, R.M., *Conceptual model for transport processes in the Culebra Dolomite Member, Rustler Formation*, SAND97-0194, Sandia National Laboratories, Albuquerque, NM, 1997.

Lafolie, F., and Ch. Hayot, One-dimensional solute transport modelling in aggregated porous media, Part 1. Model description and numerical solution, *J. Hydrol., 143*(1-2), 63-83, 1993.

Lorden, S. W., W. Chen, and L. W. Lion, Experiments and modeling of the transport of trichloroethene vapor in unsaturated aquifer material, *Environ. Sci. Technol., 32*(13), 2009-2017, 1998.

Marquardt, D. W., An algorithm for least-squares estimation of nonlinear parameters, *SIAM J. Appl. Math., 11*(2), 431-441, 1963.

McKenna, S. A., L. C. Meigs, and R. Haggerty, Tracer tests in a fractured dolomite, 4. Double porosity, multiple-rate mass transfer processes in two-well convergent flow tests, *Water Resour. Res., this issue*.

Meigs, L. C., and R. L. Beauheim, Tracer tests in a fractured dolomite, 1. Experimental design and observed tracer recoveries, *Water Resour. Res., this issue.*

Meigs L. C., S. A. McKenna, S. J. Altman, R. L.Beauheim, J. T. McCord, R. Haggerty, S. W. Flemming, T. L. Jones, J. Ogintz, and I. Farnham, *Interpretations of Tracer Tests Performed in the Culebra Dolomite at the Waste Isolation Pilot Plant Site*, *SAND97-3109,* Sandia National Laboratories, Albuquerque, NM, in review (expected publication 1999).

Neretnieks, I., Diffusion in the rock matrix: An important factor in radionuclide retardation?, *J. Geophys. Res., 85*(B8), 4379-4397, 1980.

Neretnieks, I., Solute transport in fractured rock -- Applications to radionuclide waste repositories, in *Flow and Contaminant Transport in Fractured Rock*, edited by J. Bear, C.-F. Tsang, and G. de Marsily, Academic Press, San Diego, CA, 39-127, 1993.

Pedit, J. A., and C. T. Miller, Heterogeneous sorption processes in subsurface systems, 1. Model formulations and applications, *Environ. Sci. Technol., 28*(12), 2094-2104, 1994.

Pedit, J. A., and C. T. Miller., Heterogeneous sorption processes in subsurface systems, 2. Diffusion modeling approaches, *Environ. Sci. Technol., 29*(7), 1766-1772, 1995.

Pignatello, J. J., and B. Xing, Mechanisms of slow sorption of organic chemicals to natural particles, *Environ. Sci. Technol.*, *30*(1), 1-11, 1996.

Rao, P. S. C., D. E. Rolston, R. E. Jessup, and J. M. Davidson, Solute transport in aggregated porous media: Theoretical and experimental evaluation, *Soil Sci. Soc. Am. J.*, *44*(6), 1139-1146, 1980.

Rao, P. S. C., R. E. Jessup, and T. M. Addiscott, Experimental and theoretical aspects of solute diffusion in spherical and nonspherical aggregates, *Soil Sci.*, *133*(6), 342-349, 1982.

Rasmuson, A., The effect of particles of variable size, shape and properties on the dynamics of fixed beds, *Chem. Eng. Sci.*, *40*(4), 621-629, 1985.

Ruthven, D. M., and K. F. Loughlin, The effect of crystallite shape and size distribution on diffusion measurements in molecular sieves, *Chem. Eng. Sci.*, *26*(5), 577-584, 1971.

Tsang, Y. W., Study of alternative tests in characterizing transport in fractured rocks, *Geophys. Res. Lett.*, *22*(11), 1421-1424, 1995.

Valocchi, A. J., Use of temporal moment analysis to study reactive solute transport in aggregated porous media, *Geoderma, 46*, 233-247, 1990.

van Genuchten, M. Th., and R. W. Cleary, Movement of solutes in soil: Computer-simulated and laboratory results, in *Soil Chemistry B. Physico-Chemical Models*, 2nd Edition, edited by G. H. Bolt, Elsevier Science, New York, 349-386, 1982.

Villermaux, J., Theory of linear chromatography, in *Percolation Processes, Theory and Applications*, edited by A. E. Rodrigues and D. Tondeur, *NATO ASI Ser., Ser. E, 33*, 83-140, 1981.

Wagner, B. J., and J. W. Harvey, Experimental design for estimating parameters of rate-limited mass transfer: Analysis of stream tracer studies, *Water Resour. Res.*, *33*(7), 1731-1741, 1997.

Werth, C. J., J. A. Cunningham, P. V. Roberts, and M. Reinhard, Effects of grain-scale mass transfer on the transport of volatile organics through sediments, 2. Column results, *Water Resour. Res.*, *33*(12), 2727-2740, 1997.

Wu, S., and P. M. Gschwend, Numerical modeling of sorption kinetics of organic compounds to soil and sediment particles, *Water Resour. Res.*, *24*(8), 1373-1383, 1988.

Paper 3 Figure Captions

Figure 1: Conceptual model for multirate diffusion. Although the illustrated blocks are cubes, the blocks may be of any shape. The volume of the rock shown in the diagram is less than the REV.

Figure 2: Best fits of conventional double porosity models to the H11-1 and H19S2 data. Parameters are given in Table 2.

Figure 3: Best fits of multirate diffusion model to all SWIW data. Parameters are given in Table 3.

Figure 4: Cumulative distribution functions (CDFs) estimated from each of the SWIW data. CDFs shown here correspond to the models shown in Figure 3 and the parameters given in Table 3.

Figure 5: Normalized sensitivity for estimated parameters of multirate diffusion model at H11-1 and at H19S2.

Figure 6: Sensitivity analysis for σ_d (standard deviation of $\ln(\alpha_d)$) in multirate diffusion model. The curve for $\sigma_d = 0$ is equivalent to the conventional double porosity model.

parameter:	test:				
	H11-1	H11-2	H19S2	H19S1-1	H19S1-2
solute injection time [s]	8.16E+03	7.98E+03	7.32E+03	7.62E+03	7.95E+03
chaser injection time [s]	1.54E+04	7.44E+03	1.46E+04	1.58E+04	7.83E+03
pause length, t_{rest} [s]	6.36E+04	6.36E+04	6.38E+04	6.22E+04	6.22E+04
injection rate, Q_{inj} [m^3/s]	1.22E-04	1.27E-04	1.16E-04	1.31E-04	1.26E-04
pumping rate, Q_{out} [m^3/s]	2.24E-04	2.24E-04	2.74E-04	2.37E-04	2.37E-04
well radius, r_w [m]	0.065	0.065	0.113	0.113	0.113
thickness, b [m]	4.4	4.4	4.4	4.4	4.4
matrix porosity, ϕ_d [-]	0.160	0.160	0.147	0.147	0.147
grid radius [m]	8.00	8.00	3.75	3.75	3.75

Table 1: Fixed parameters used in simulations.

Test	Log[mean (D_e/a^2)] μ_d	Advective Porosity ϕ_a [-]	Dispersivity α_L [-]	RMSE
H19S2	-16.2	0.0540	0.159	1.27
H11-1	-18.8	0.00714	0.458	0.527

Table 2: Single-rate double porosity estimation results.

Test	Log[mean (D_e/a^2)] $\mu_d \pm 2\sigma$ range	Std. Dev. Log(D_e/a^2) σ_d $ln(\sigma_d) \pm 2\sigma$ range	Advective Porosity ϕ_a [-] $ln(\phi_a) \pm 2\sigma$ range	Dispersivity α_L [m] $ln(\alpha_L) \pm 2\sigma$ range	RMSE
H11-1	-15.8 ± 1.09 -14.7, -16.9	3.55 *1.27 ± 0.245* 2.79, 4.54	0.00175 *-6.35 ± 4.59* 1.77E-05, 0.174	0.0566 *-2.87 ± 4.35* 7.33E-04, 4.37	0.151
H11-2	-15.7 ± 0.942 -14.7, -16.6	3.83 *1.34 ± 0.238* 3.02, 4.858	0.00430 *-5.45 ± 2.53* 3.43E-04, 0.0538	0.0365 *-3.31 ± 5.08* 2.28E-04, 5.84	0.152
H19S2	-10.9 ± 1.67 -9.23, -12.5	5.83 *1.76 ± 0.237* 4.60, 7.38	0.0151 *-4.19 ± 2.74* 9.78E-04, 0.233	0.173 *-1.76 ± 0.237* 0.136, 0.219	0.161
H19S1-1	-11.9 ± 3.96 -7.94, -15.9	6.87 *1.93 ± 0.297* 5.12, 9.272	0.00485 *-5.33 ± 12.8* 1.34E-08, >1	0.213 *-1.55 ± 0.356* 0.149, 0.303	0.276
H19S1-2	-10.1 ± 3.98 -6.12, -14.1	2.56 *0.940 ± 0.822* 1.13, 5.83	0.0202 *-3.90 ± 12.7* 6.18E-08, >1	0.117 *-2.15 ± 1.80* 0.019, 0.705	0.424

Table 3: Multirate estimation results. For a given test, 1st row in each column (except that for μ_d) gives the best-fit parameter value; 2nd row gives the natural logarithm of the best-fit parameter value and 95% confidence limits; and 3rd row gives the range of possible parameter values to within 95% confidence. μ_d was directly estimated (as opposed to its logarithm), so confidence limits are given in arithmetic space. See text for details.

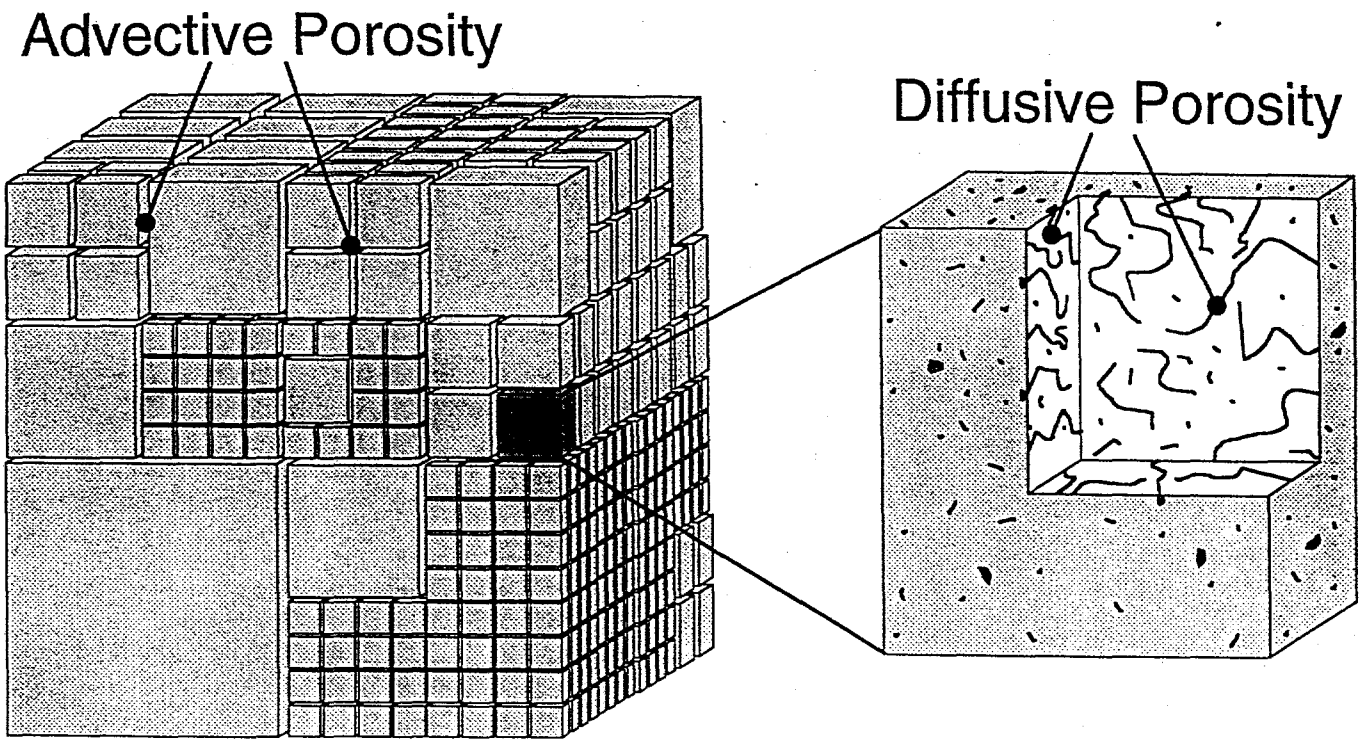

Fig. 1

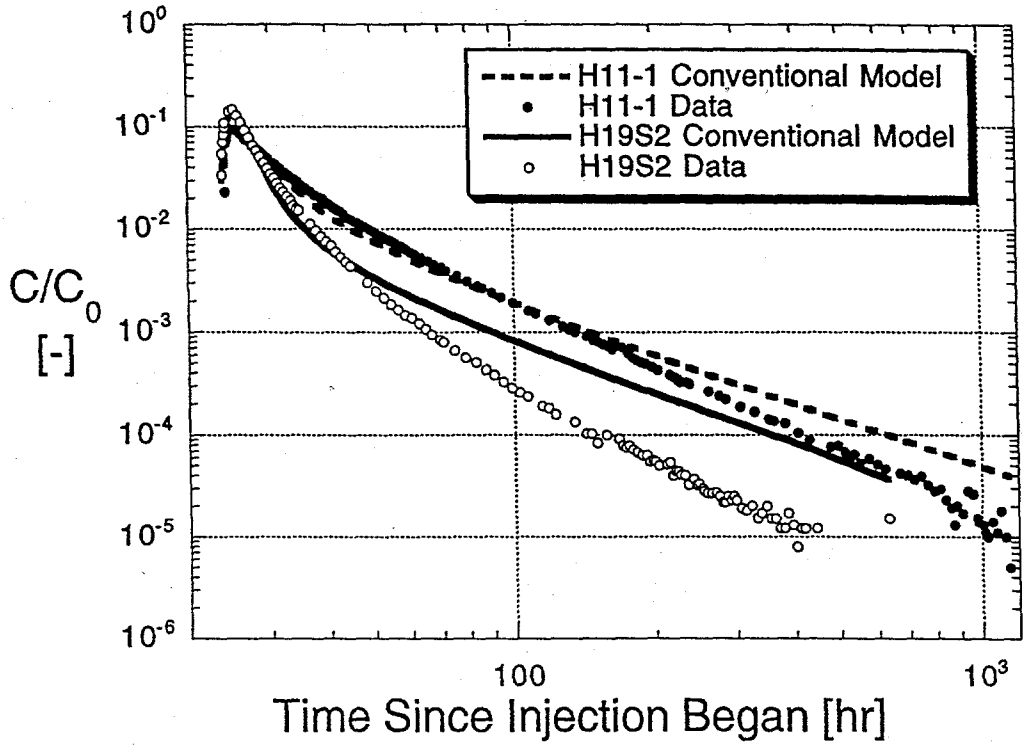
H11-1 Conventional Model
H11-1 Data
H19S2 Conventional Model
H19S2 Data
C/C0
[-]
10^0
10^-1
10^-2
10^-3
10^-4
10^-5
10^-6
100
10^3
Time Since Injection Began [hr]

Fig. 2

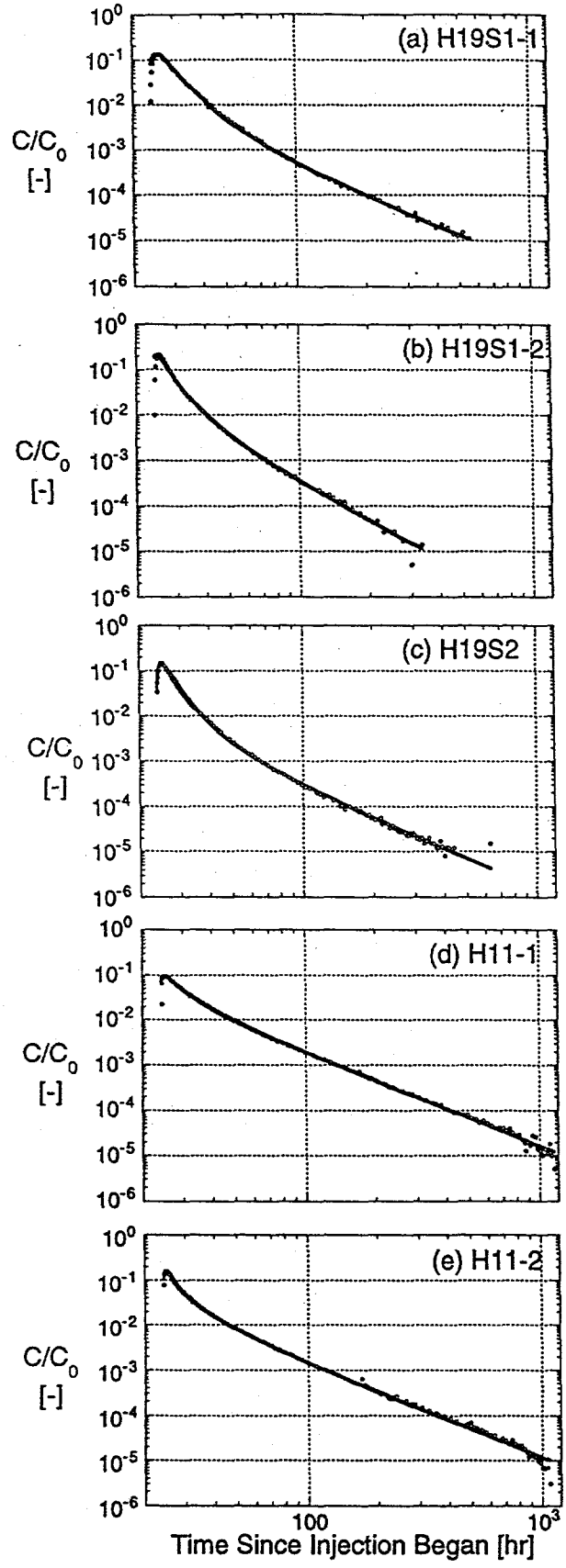
(a) H19S1-1
(b) H19S1-2
(c) H19S2
(d) H11-1
(e) H11-2
C/C0 [-]
10^0
10^-1
10^-2
10^-3
10^-4
10^-5
10^-6
100
10^3
Time Since Injection Began [hr]

Fig. 3

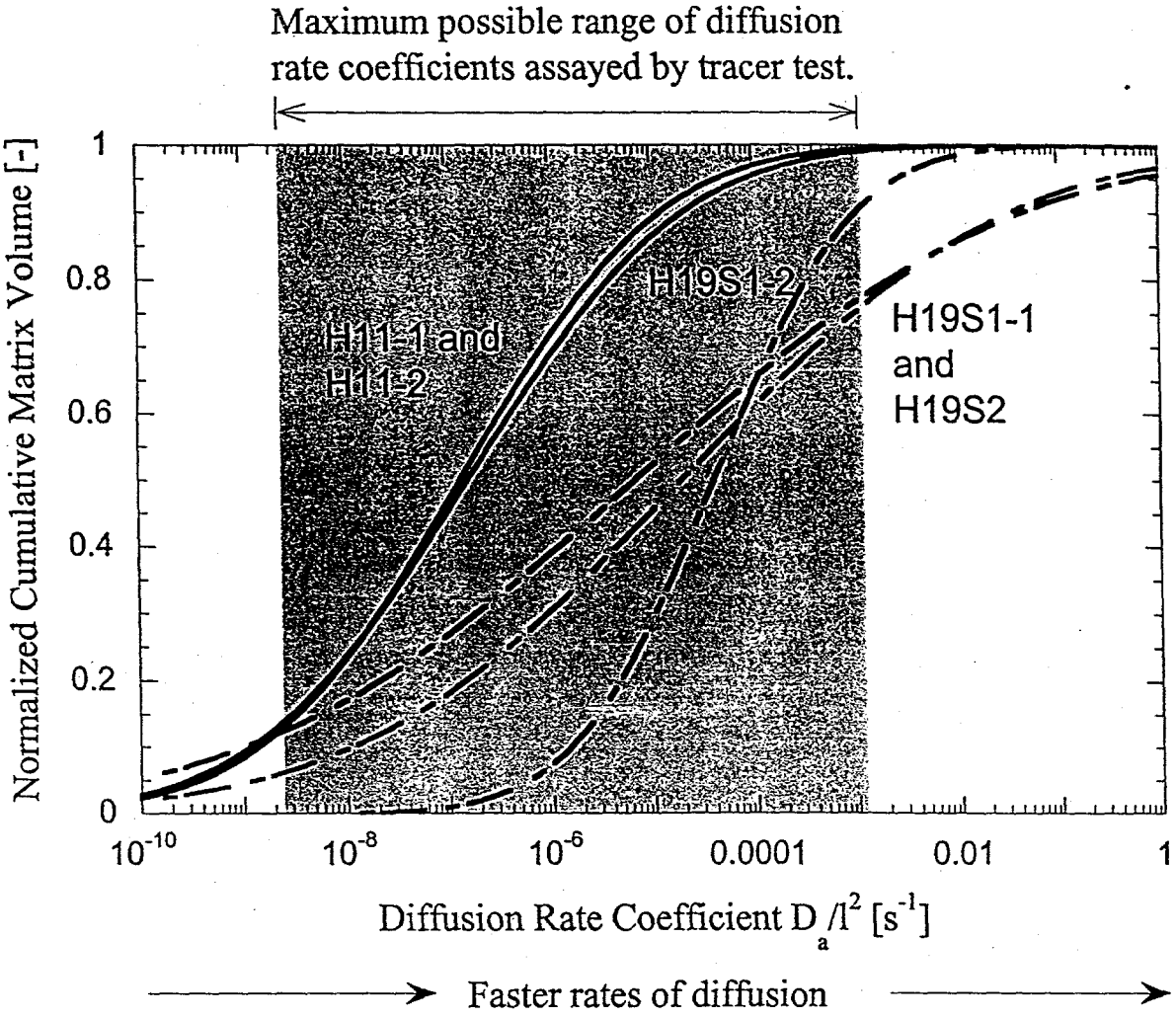
Maximum possible range of diffusion rate coefficients assayed by tracer test.
Normalized Cumulative Matrix Volume [-]
1
0.8
0.6
0.4
0.2
0
H19S1-2
H11-1 and H11-2
H19S1-1 and H19S2
10-10
10-8
10-6
0.0001
0.01
1
Diffusion Rate Coefficient Da /l2 [s-1]
Faster rates of diffusion

Fig. 4

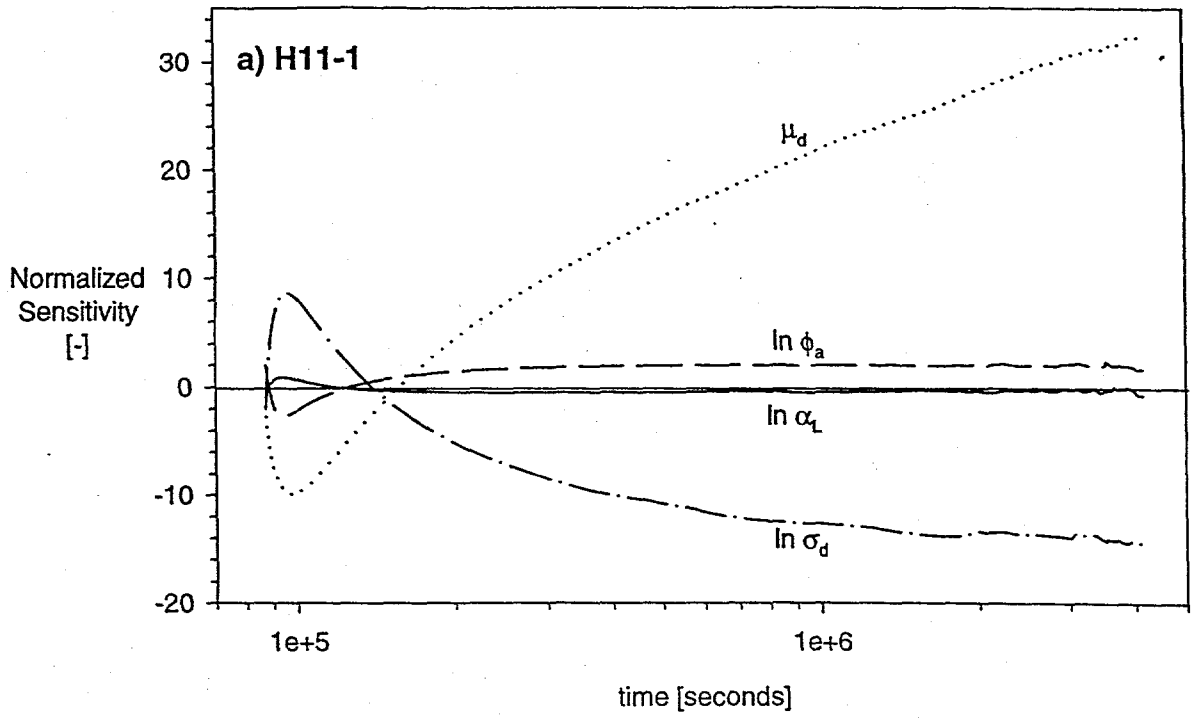

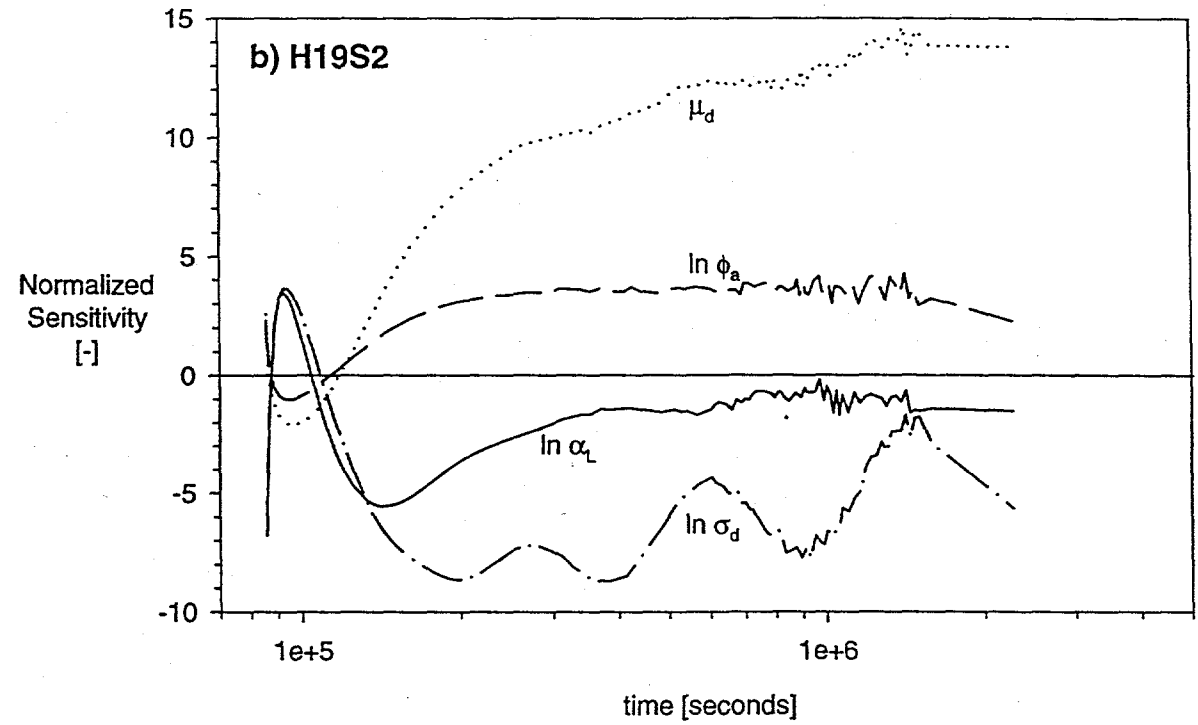

FIGURE5.JNB; indices: h19S2.110698-03, h11-1.110698-01

Fig 5

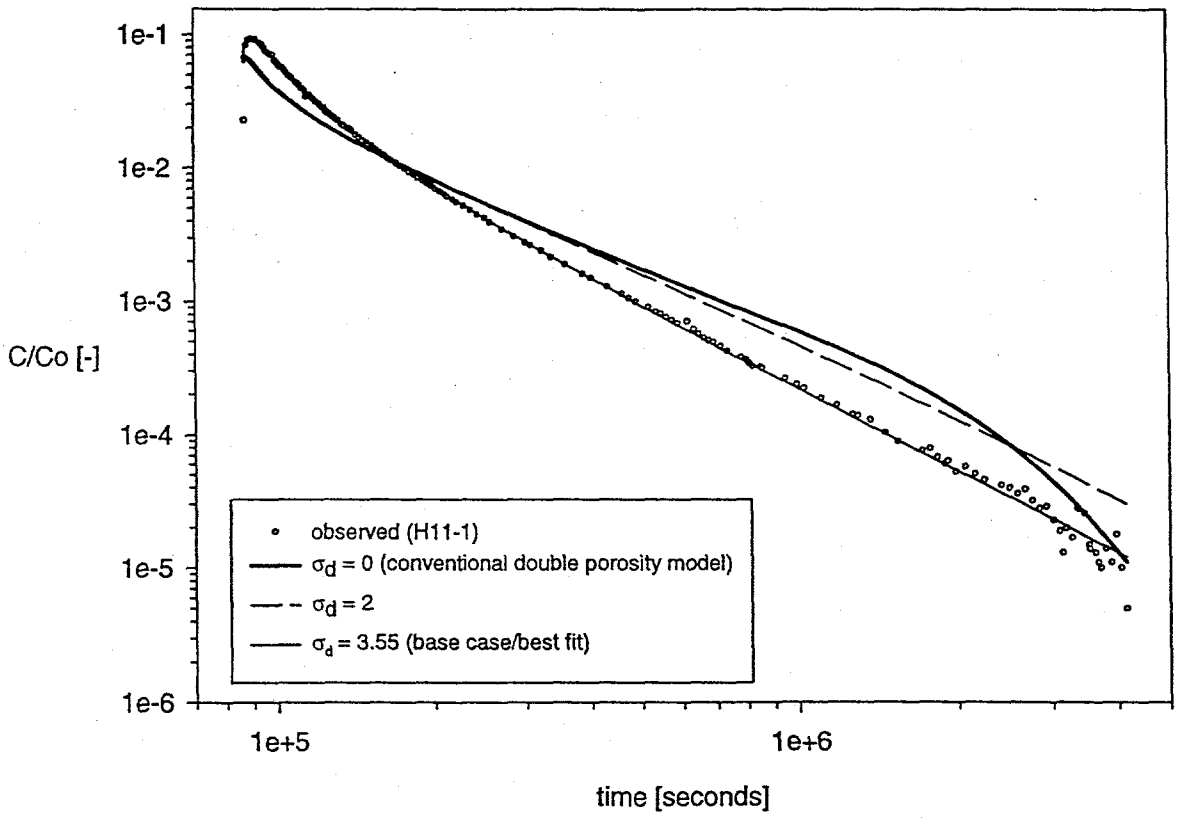

FIGURE6.JNB; indices: h11-1.170698-02, h11-1.180698-01, h11-1.180698-02

Fig. 6